Molecular Therapy
Nucleic Acids
Original Article

Adeno-associated virus-mediated delivery of anti-miR-199a tough decoys attenuates cardiac hypertrophy by targeting *PGC-1alpha*

Hualin Yan,[1] Hong Wang,[1] Xiaoxia Zhu,[1] Jianbo Huang,[1] Yifei Li,[2,3] Kaiyu Zhou,[2,3] Yimin Hua,[2,3] Feng Yan,[1] Da-Zhi Wang,[4] and Yan Luo[1]

[1]Department of Medical Ultrasound, Laboratory of Ultrasound Imaging Drug, West China Hospital, Sichuan University, Chengdu 610041, China; [2]Department of Pediatrics, West China Second University Hospital, Sichuan University, Chengdu 610041, China; [3]Ministry of Education Key Laboratory of Women and Children's Diseases and Birth Defects, West China Second University Hospital, Sichuan University, Chengdu 610041, China; [4]Department of Cardiology, Boston Children's Hospital, Harvard Medical School, 300 Longwood Avenue, Boston, MA 02115, USA

MicroRNAs (miRNAs) are important regulators in the process of cardiac hypertrophy and heart failure. Previous studies have shown that miR-199a is upregulated in pressure-overload cardiac hypertrophy and that inhibition of miR-199a attenuates cardiac hypertrophy *in vitro*. However, the therapeutic role of anti-miR-199a treatment in the cardiac hypertrophy *in vivo* model is less known. Here, we show an efficient and useful method to treat mouse cardiac hypertrophy and restore cardiac function through injection of adeno-associated virus (AAV)-mediated anti-miR-199a tough decoys (TuDs). RNA-seq transcriptome analysis indicated that genes related to cytoplasmic translation and mitochondrial respiratory chain complex assembly were upregulated in anti-miR-199a-treated recovered hearts. We further validated that PGC-1α is the direct target of miR-199a involved in the therapeutic effect and the regulation of the PGC-1α/ERRα axis and that the downstream pathway of mitochondrial fatty acid oxidation and oxidative phosphorylation constitute the underlying mechanism of the restored mitochondrial structure and function in our anti-miR-199a-treated mice. Our study highlights the important regulatory role of miR-199a in cardiac hypertrophy and the value of the AAV-mediated miRNA delivery system.

INTRODUCTION

Pathological cardiac hypertrophy is a compensatory cardiac remodeling response characterized by cardiac enlargement and cardiomyocyte hypertrophy in response to neurohormonal stimulation and mechanical forces under pathological conditions. Prolonged exposure to stress stimuli causes cardiac remodeling to become maladaptive decompensation, accompanied by the following processes: cell death, fibrosis, dysregulation of Ca^{2+}-handling proteins, mitochondrial dysfunction, metabolic reprogramming, increase of reactive oxygen species, and altered sarcomere structure.[1] Among them, mitochondrial dysfunction and metabolic remodeling can be the direct cause of pathological cardiac hypertrophy.[1] Mitochondrial biogenesis, metabolic reprogramming (changes in fatty acid oxidation [FAO] and glycolysis pathway), mitochondrial oxidative stress, and oxidative phosphorylation (OXPHOS) have been shown to associated with pathological cardiac hypertrophy.[2–6]

MicroRNAs (miRNAs) are a class of small, noncoding RNAs that regulate gene expression at the post-transcription level. Growing evidence has shown that miRNAs play important roles in the progression of cardiac hypertrophy[7–10] and they can regulate cardiac mitochondrial dysfunction, which results in pathological cardiac hypertrophy and heart failure (HF).[2–4,6,11] The manipulation of these miRNAs can be a therapeutic strategy to treat cardiac hypertrophy. However, common chemically modified miRNAs, such as miRNA agomirs/antagomirs, miRNA mimics, and miRNA sponges, have transient lifespans with short-term effects and require large-dose and repetitive delivery.[12] Recent studies demonstrated that adeno-associated virus (AAV)-mediated delivery of miRNA interference sequence *in vivo* achieved efficient and persistent therapeutic effects on cardiovascular diseases.[7,8,13–15] Compared with chemically modified miRNAs, AAV9 has high tropism for the heart, and miRNA interference sequence expression can be cell specific when we used cardiac-specific promoter, such as cTNT or α-MHC.[12,16] In addition, AAV exhibits long-term (25 weeks) effects of miRNA intervention and is safe, without adverse side effects.[12,17]

Our previous study found that miR-199a was upregulated in isoproterenol (ISO)-induced cardiac hypertrophy.[18] miR-199a was identified as an important regulator in primary cardiomyocyte hypertrophy.[19] The inhibitory effect of miR-199a on hypertrophic primary cardiomyocytes results in reduced cell size and attenuated hypertrophy.[20] We hypothesize that the *in vivo* inhibition of miR-199a in a

Received 5 September 2020; accepted 10 November 2020;
https://doi.org/10.1016/j.omtn.2020.11.007.

Correspondence: Yan Luo, Department of Medical Ultrasound, Laboratory of Ultrasound Imaging Drug, West China Hospital, Sichuan University, No. 37, Guoxue Xiang, Chengdu, Sichuan 610041, China.
E-mail: luoyanddoc@163.com

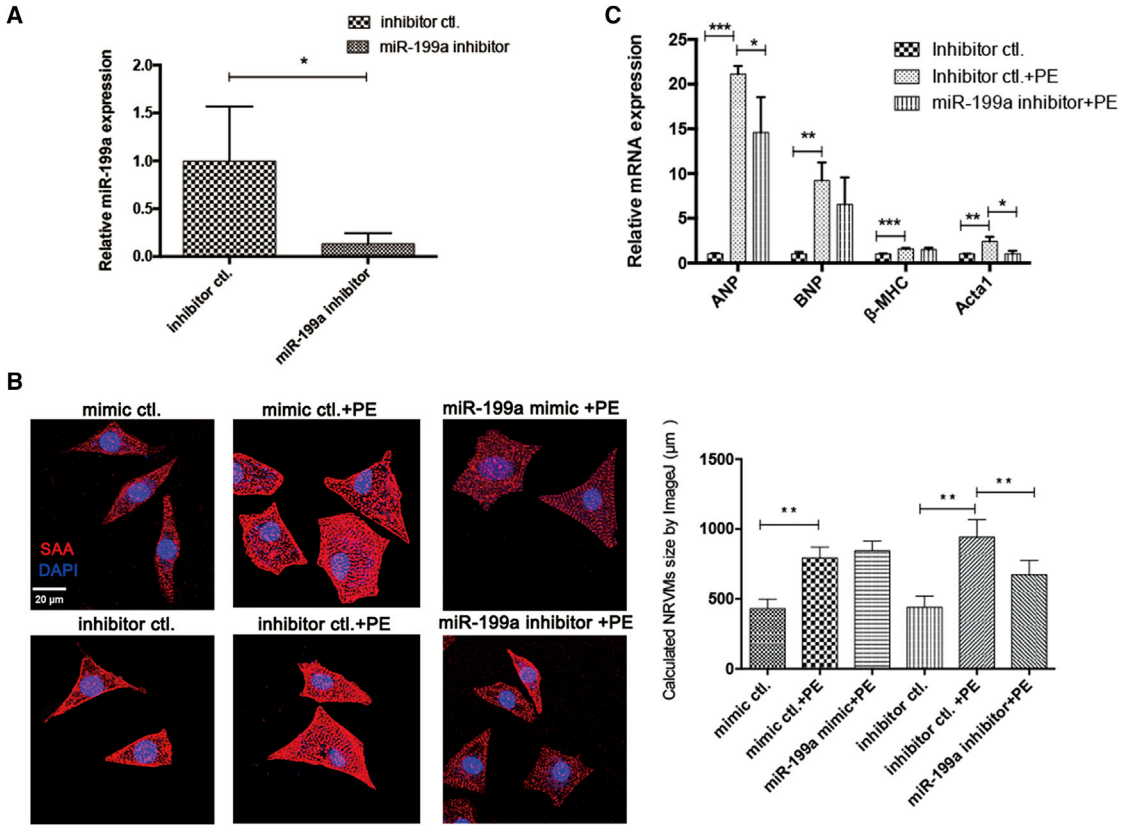

Figure 1. Inhibition of miR-199a attenuated hypertrophy of neonatal rat ventricular cardiomyocytes

(A) The expression of miR-199a in NRVMs with or without miR-199a inhibitor treatment (n = 3). (B) Representative confocal images of sarcomeric alpha actinin (SAA, red) and DAPI (nuclei, blue) staining of NRVMs in different groups. NRVM size in each group was calculated by ImageJ. Scale bar, 20 μm. Approximately 200 counted cells in each group. (C) The expression of hypertrophic markers ANP, BNP, β-MHC, and Acta1 in each NRVM group (n = 3). *p < 0.05, **p < 0.01, ***p < 0.001.

cardiac hypertrophy model through AAV delivery can result in amelioration of cardiac hypertrophy and restored cardiac function. Here, we aimed to investigate the role of miR-199a in pathological cardiac hypertrophy through AAV-mediated miRNA delivery and to achieve therapeutic effects on cardiac hypertrophy and heart function.

RESULTS

Inhibition of miR-199a attenuated hypertrophy of neonatal rat ventricular cardiomyocytes (NRVMs)

The expression level of miR-199a in NRVMs was significantly decreased to 13% in the inhibitor group compared with the control group (Figure 1A). Based on the calculated cardiomyocyte size in each group, inhibition of miR-199a by the miR-199a inhibitor significantly reduced the cardiomyocyte size of hypertrophic NRVMs, while overexpression of miR-199a by the miR-199a mimic did not change the size of hypertrophic cardiomyocytes (Figure 1B). The elevated hypertrophic markers ANP and Acta1 were significantly decreased by inhibition of miR-199a, while BNP and β-MHC were not significantly changed after inhibition of miR-199a (Figure 1C).

AAV9 technology enabled safe, cardiac-specific, and highly efficient cardiac infection and long-term miR-199a inhibition *in vivo*

The injection of AAV9-anti-miR-199a tough decoys (TuDs) or AAV9-cTNT-EGFP virus (1×10^{11} viral genomes [Vg] per neonatal mouse) achieved a very high infection efficiency since 8 days of age (Figures 2A and 2B). Calculated by the percentage of GFP that both AAV viruses expressed, the average infection efficiency of AAV9-anti-miR-199a TuDs and AAV9-cTNT-EGFP virus was 30% and 24% at 8 days of age, respectively, and both AAVs sustained high expression until 13 weeks of age (Figure 2C). The high and sustained expression of AAV9-anti-miR-199a TuDs virus achieved stable inhibition of miR-199a in the heart throughout the observation period (Figure 2D). As AAV expression was driven by the cardiac-specific cTNT promoter, the expression was almost absent in other organs, such as the liver, brain, and skeletal muscle of the injected mice (Figure 2E), and miR-199a expression was not inhibited in liver, brain, and skeletal muscle of the injected mice (Figure 2F).

Moreover, AAV was safe in terms of the systemic inflammatory response. The inflammatory cytokines interleukin-1β (IL-1β), IL-6,

and interferon-γ (IFN-γ) showed no significant increase in the serum of the injected mice compared with that in wild-type mice (Figure 2G).

Injection of AAV9-anti-miR-199a TuDs virus alleviated cardiac hypertrophy and restored cardiac function *in vivo*

The injection of AAV9-anti-miR-199a TuDs virus significantly reduced the hypertrophic cardiac size induced by ISO (Figure 3A). The cardiac hypertrophy index, the ratio of heart weight and tibia length, significantly decreased to normal value (Figure 3B). Treatment with AAV9-anti-miR-199a TuDs virus significantly reduced the hypertrophic cardiomyocyte size calculated from the wheat germ agglutinin (WGA) staining (Figure 3C). Furthermore, miR-199a inhibition treatment restored cardiac function. The left ventricular ejection fraction (LVEF) of treated mice increased to 72%, and the left ventricular fractional shortening (LVFS) of treated mice increased to 40%, significantly (Figure 3D; detailed echocardiographic assessment in Table S1). The cardiac hypertrophy markers ANP, BNP, and Acta1 were all dramatically reduced after miR-199a inhibition treatment (Figure 3E). However, the cardiac fibrosis and apoptosis were not significantly changed after anti-miR-199a treatment (Figures S1 and S2). Overall, miR-199a inhibition treatment by AAV9-anti-miR-199a TuDs virus not only attenuated cardiac hypertrophy but also restored heart function of cardiac hypertrophy mice.

As shown by the efficiency of AAV in mice without cardiac hypertrophy (Figure 2D), the elevated expression level of miR-199a in the cardiac hypertrophy model was significantly decreased by AAV9-anti-miR-199a TuDs virus (Figure 3F), which was the basis for the therapeutic effect against cardiac hypertrophy and cardiac dysfunction. However, AAV9-anti-miR-199a TuDs virus treatment had no effect on the expression of miR-199b (Figure S3).

RNA-seq revealed the possible underlying protective mechanism of anti-miR-199a treatment in cardiac hypertrophy

To better understand the molecular mechanisms underlying anti-miR-199a-mediated effects against cardiac hypertrophy, we performed next-generation RNA sequencing (RNA-seq) in AAV9-anti-miR-199a TuDs-treated and AAV9-EGFP control heart samples. Compared to the control samples, a total of 2,429 genes were significantly upregulated, and 2,619 genes were significantly downregulated (Figure 4A). Gene Ontology (GO) enrichment analysis revealed that genes related to cytoplasmic translation, mitochondrial respiratory chain complex assembly, and ribonucleoprotein complex biogenesis were enriched among anti-miR-199a-upregulated genes (Figure 4B). Kyoto Encyclopedia of Genes and Genomes (KEGG) pathway analysis revealed that the ribosome pathway and OXPHOS pathway are the main pathways involved (Figure 4C). Further PCR validation showed that representative ribosome genes Rps27a, Mrps21, and Mrpl14 all increased significantly after anti-miR-199a treatment, indicating active translation in the anti-miR-199a-treated group (Figure 4D). Representative genes involved in OXPHOS, Ndufa6, Sdhb, Uqcrh, Uqcrq, Cox4i1, and Atp5l, all increased significantly after anti-miR-199a treatment in the cardiac hypertrophy model (Figure 4E), suggesting that OXPHOS and the related mitochondrial metabolism pathways constitute a possible underlying mechanism of the anti-miR-199a protective effect.

Target prediction and validation of miR-199a in cardiac hypertrophy *in vitro* and *in vivo*

Through the target prediction results in TargetScan v7.2 (http://www.targetscan.org/) and TarBase v7.0 (http://diana.imis.athena-innovation.gr/DianaTools/index.php?r=tarbase/index) and the reported validated miR-199a targets in heart diseases,[4,21–23] we chose six potential targets related to mitochondrial metabolism or cardiac hypertrophy for further study (Table 1). Among these six potential targets, Ppargc1a (PGC-1α) was the only target that was derepressed after inhibition of miR-199a both *in vitro* and *in vivo* (Figures 5A and 5B). The nucleotide position 1518–1525 of the 3′UTR of the Ppargc1a gene was the predicted binding site of miR-199a, and it was conserved across different species (Figure 5C). Furthermore, a dual luciferase reporter assay showed that the miR-199a mimic significantly inhibited the luciferase activity of the Luc-PGC-1α-3′UTR reporter plasmid, while the luciferase activity remained unchanged in the mutant plasmid or miRNA mimic control group (Figure 5D), which suggests that PGC-1α is a direct target of miR-199a.

Anti-miR-199a treatment attenuated cardiac hypertrophy via PGC-1α and the mitochondrial metabolic pathway

Through transmission electron microscopy (TEM), the mitochondrial ultrastructure was found to be disrupted in hypertrophic cardiomyocytes, while anti-miR-199a treatment attenuated mitochondrial network disorganization and maintained their linear array (Figure 6A).

To explore the altered genes related to mitochondrial metabolism, we detected the expression levels of genes involved in glycolysis and FAO and important transcription factors involved in mitochondrial metabolism. Glucose transporter 1 (Glut1) and glucose transporter 4 (Glut4) are important uniporter proteins that facilitate the transport of glucose across cell membranes. Hexokinase 1 (Hk1) is the rate-limiting enzyme that catalyzes glucose into glucose-6-phosphate (G-6-P). Glut1, Glut4, and Hk1 levels all returned to normal expression levels upon miR-199a inhibition, indicating restored glycolysis in treated mice (Figure 6B). In the FAO pathway, Cd36, or fatty acid translocase, imports fatty acids inside cells. Carnitine palmitoyl transferase Ib (Cpt1b), acyl-coenzyme A oxidase 1 (Acox1), acyl-coenzyme A dehydrogenase medium chain (Acadm), and acyl-CoA dehydrogenase very long chain (Acadvl) are all important fatty acid beta-oxidation enzymes. The expression levels of Acox1 and Cpt1b were restored after anti-miR-199a treatment, and Acadm and Acadvl even increased to approximately twice the normal expression levels, suggesting activated FAO (Figure 6C).

Crucial transcription factors in mitochondrial metabolism, ERRα, PPARα, and PGC-1α, were restored upon anti-miR-199a treatment (Figure 6D). The corresponding protein levels of ERRα and PGC-1α were consistent with the mRNA changes induced by miR-199a inhibition (Figure 6E).

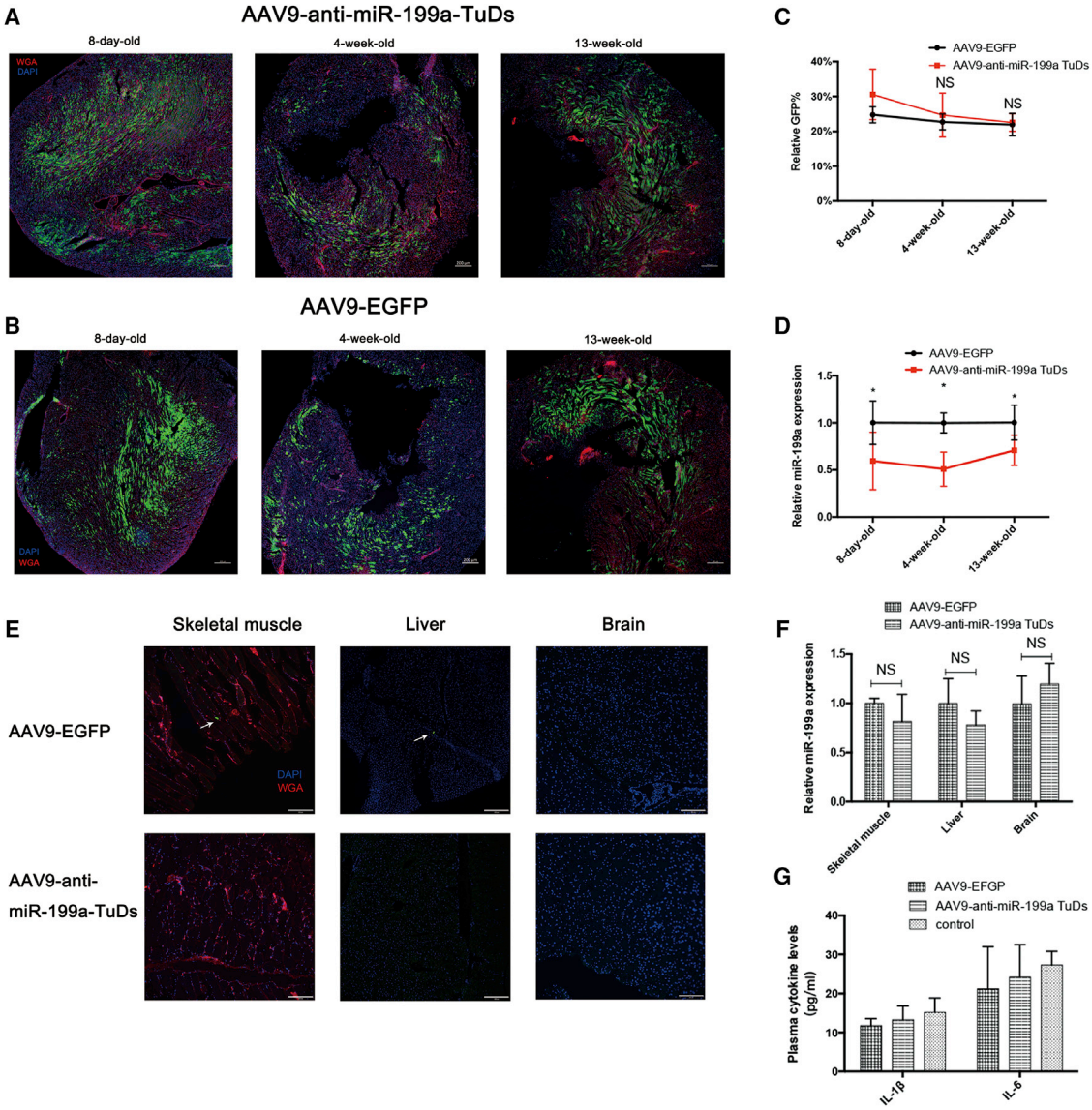

Figure 2. AAV-mediated miR-199a inhibition *in vivo*

(A and B) Representative confocal images of wheat germ agglutinin (WGA, red) and DAPI (nuclei, blue) staining of hearts in 8-day-old, 4-week-old, and 13-week-old mice injected with AAV9-anti-miR-199a TuDs or AAV9-EGFP. Green, autofluorescence of cardiomyocytes with AAV9 virus infection. Scale bars, 200 μm; n = 4–5. (C) Calculated relative percentage of GFP-positive cells in the hearts of 8-day-old, 4-week-old, and 13-week-old mice injected with AAV9-anti-miR-199a TuDs or AAV9-EGFP. n = 4–5 different sections in each group. NS represents not significant compared with that in 8-day-old mice. (D) The expression of miR-199a in the hearts of 8-day-old, 4-week-old, and 13-week-old mice injected with AAV9-anti-miR-199a TuDs or AAV9-EGFP (n = 6). (E) Representative confocal images of WGA (red) and DAPI (nuclei, blue) staining of skeletal muscle, liver, and brain tissue in 13-week-old mice injected with AAV9-anti-miR-199a TuDs or AAV9-EGFP. Arrow, green autofluorescence of cardiomyocytes with AAV9 infection. Scale bars, 200 μm; n = 3. (F) The expression of miR-199a in liver, brain, and skeletal muscle of 13-week-old mice with AAV9-anti-miR-199a TuDs or AAV9-EGFP injection (n = 5). NS, not significant. (G) The plasma cytokine levels of IL-1β, IL-6, and IFN-γ in AAV-injected mice and wild-type control mice (n = 6). IFN-γ in each group was lower than 7.8 pg/mL. *$p < 0.05$, **$p < 0.01$.

DISCUSSION

In the present study, we successfully ameliorated mouse cardiac hypertrophy and cardiac dysfunction by injection of AAV9-anti-miR-199a TuDs. RNA-seq indicated that OXPHOS and the related mitochondrial metabolic pathway constituted the possible mechanism underlying this therapeutic phenotype. Furthermore, we confirmed that PGC-1α was the direct target of miR-199a involved in this pathway. Our results revealed that the regulation of the PGC-1α/ERRα axis and the downstream pathway of mitochondrial FAO and OXPHOS is the underlying mechanism of the restored mitochondrial structure and function in our anti-miR-199a-treated mice.

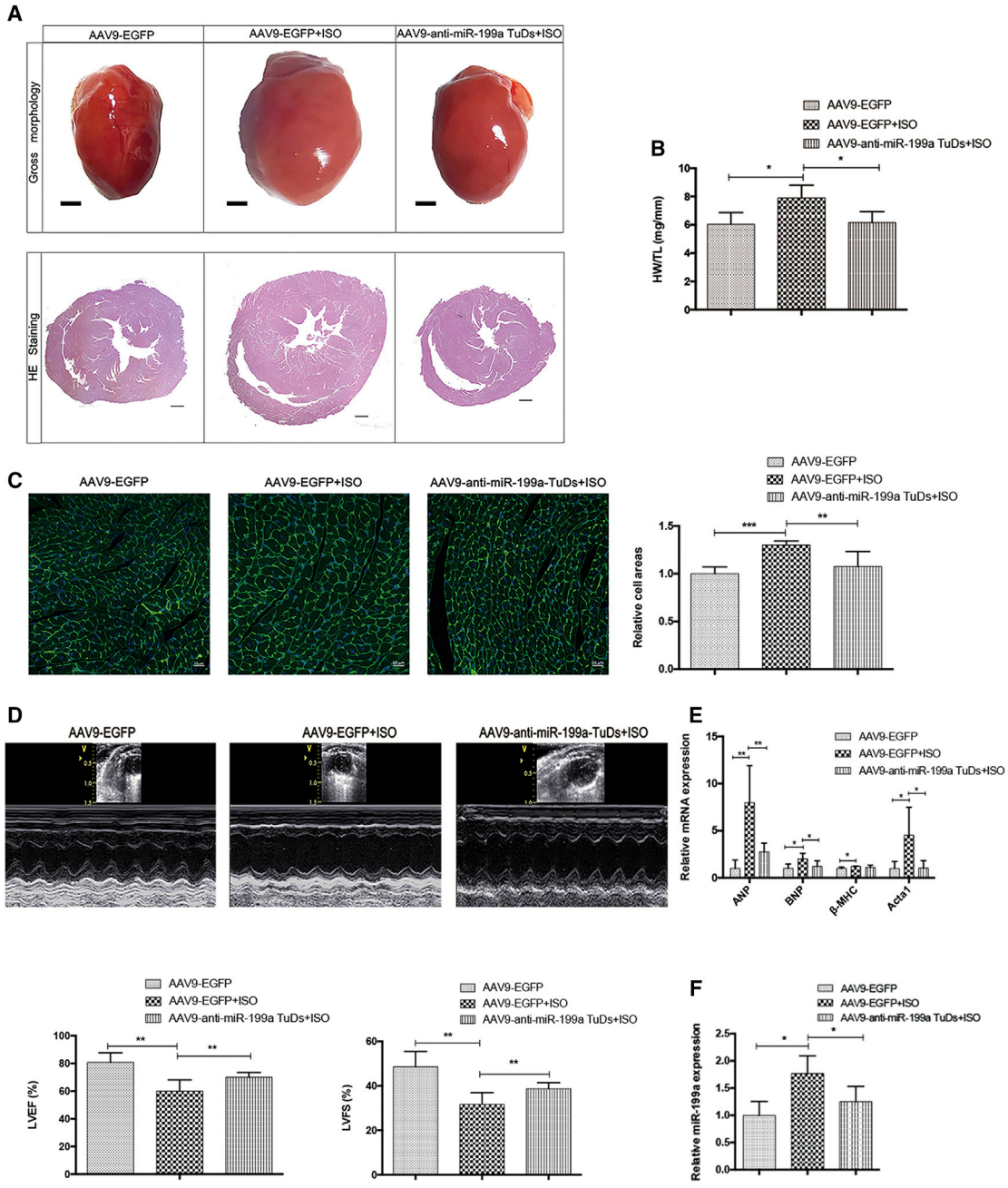

Figure 3. AAV9-anti-miR-199a TuDs virus attenuated cardiac hypertrophy

(A) The representative gross morphology (scale bars, 1 mm) and H&E staining (scale bars, 400 μm) of heart sections in control and cardiac hypertrophy mice injected with AAV9-anti-miR-199a TuDs or AAV9-EGFP. n = 8. (B) The ratio of heart weight (HW, mg) and tibia length (TL, mm) in different mouse groups. n = 8. (C) Representative images of WGA (green) and DAPI (nuclei, blue) staining of hearts in different mouse groups (left). Scale bars, 20 μm. Calculated relative cell areas of cardiomyocytes in different mouse groups (right). n = 8. (D) Representative M-mode echocardiography images in different mouse groups (top). The percentages of left ventricular ejection fraction (LVEF) and left ventricular fractional shortening (LVFS) in the different mouse groups (bottom). n = 8. (E) The expression of hypertrophic markers ANP, BNP, β-MHC, and Acta1 in different mouse groups. n = 8. (F) The expression of miR-199a in different mouse groups. n = 8 in each group. *$p < 0.05$, **$p < 0.01$, ***$p < 0.001$.

The PGC-1/ERR axis has been considered a candidate therapeutic target for pathological cardiac hypertrophy and heart failure for decades.[24] Growing evidence supports that the PGC-1/ERR axis plays a key role in myocardial mitochondrial metabolism and pathological cardiac hypertrophy. The cardiac-specific knockout (KO) of PGC-1α in mice induces suppressed glucose oxidation and FAO, decreased

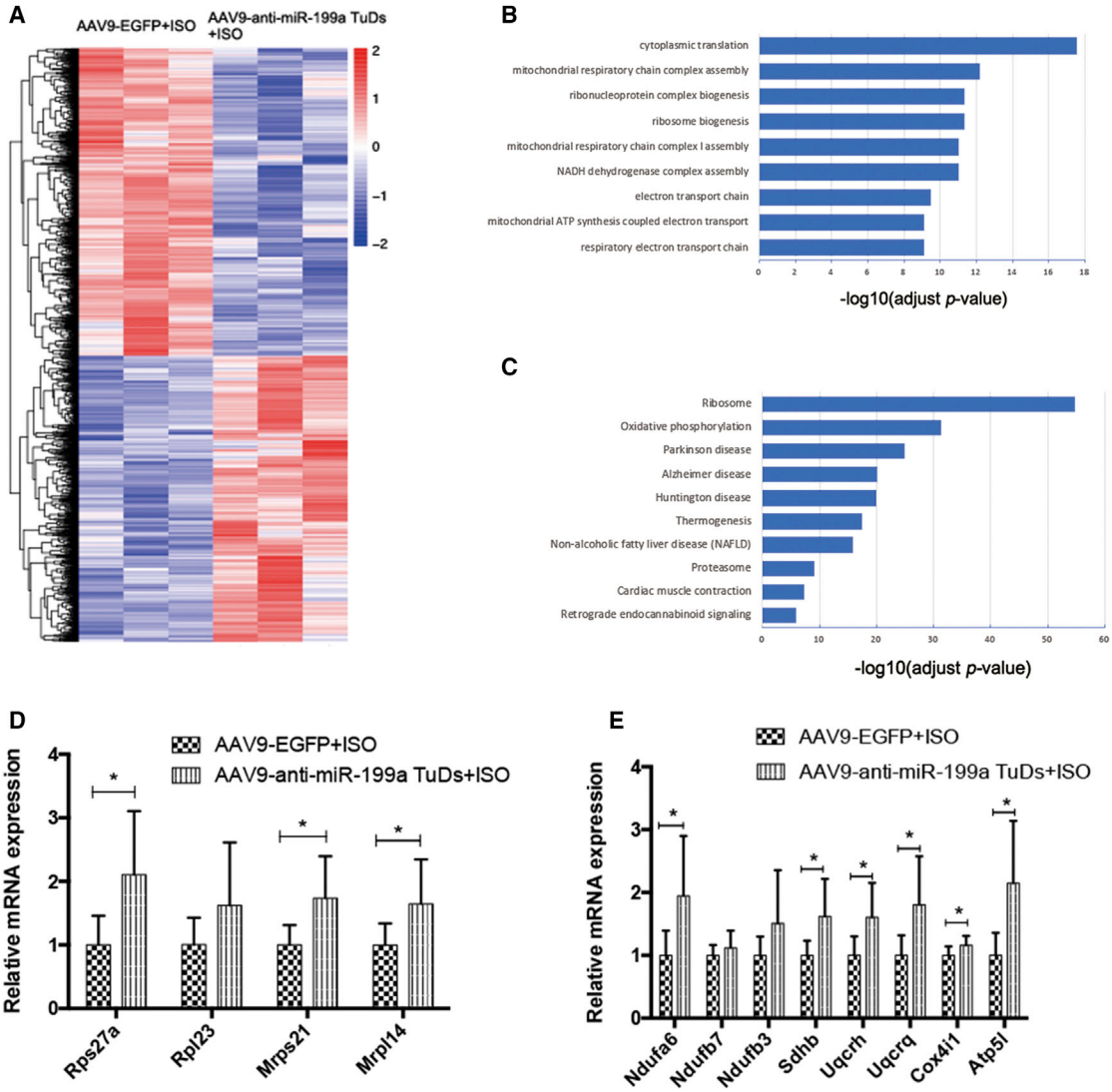

Figure 4. RNA sequencing results of anti-miR-199a treatment in cardiac hypertrophy

(A) Heatmap of all genes with significantly altered expression between the cardiac hypertrophy group and the anti-miR-199a-treated group. Red and blue colors indicate upregulated or downregulated genes. n = 3 per group. (B) Gene Ontology (GO) enrichment analysis of all significantly upregulated genes. The y axis shows the top 10 enriched pathways. The x axis is the −log10 of the adjusted p value. (C) Kyoto Encyclopedia of Genes and Genomes (KEGG) analysis of all significantly upregulated genes. The y axis shows the top enriched pathways. The x axis is the −log10 of the adjusted p value. (D) The expression of representative ribosome genes in the cardiac hypertrophy group and the anti-miR-199a-treated group. n = 8. (E) The expression of representative genes involved in oxidative phosphorylation in the cardiac hypertrophy group and the anti-miR-199a-treated group. n = 8 per group. *$p < 0.05$, **$p < 0.01$.

OXPHOS, and reduction in mitochondrial density, which leads to dilating cardiomyopathy and heart failure.[25] The lack of PGC-1α also accelerated transverse aortic constriction (TAC)-induced heart failure with decreased FAO and OXPHOS.[26] However, the cardiac-specific overexpression of PGC-1α in mice resulted in mitochondrial ultrastructural abnormalities and dilating cardiomyopathy, which was reversible after cessation of PGC-1α overexpression.[27,28] Interestingly, PGC-1α acts in a developmental stage-dependent manner: the induction of PGC-1α in the neonatal heart leads to dramatic mitochondrial biogenesis, while the induction of PGC-1α in adult mice causes mitochondrial structural derangements and cardiomyopathy.[28] These findings explain why maintaining PGC-1α expression through a transgenic mouse model failed to attenuate pressure-overload cardiac hypertrophy and improve cardiac function[29,30]. In our study, the derepression of PGC-1α by miR-199a inhibition was modest, with only 1.3-fold change compared with that in control mice (Figure 6D). In addition, PGC-1α may not be the only target of miR-199a involved in mitochondrial recovery and cardiac relief.

Table 1. Predicted targets of miR-199a in cardiac hypertrophy

Predicted target gene	Representative transcript in *Mus musculus*	Gene name	Site in untranslated regions (UTR) (Lower row is the sequence of mmu-miR-199a)		Reported pathway in cardiac hypertrophy and heart failure
Ppargc1a	NM_008904.2	peroxisome proliferative activated receptor, gamma, coactivator 1 alpha	Position 1518-1525 of Ppargc1a 3' UTR	5' ...UCUUUGAAGUUUUAUACACUGGA... 3' CUUGUCCAUCAGACU-UGUGACCC	mitochondrial biogenesis[28], cardiac metabolic remodeling[25]
Dyrk1a	NM_001113389.1	dual specificity tyrosine-phosphorylation-regulated kinase 1A	Position 1547-1554 of Dyrk1a 3' UTR	5' ...UCUGAAGGGAAAGGGACACUGGA... 3' CUUGUCCAUCAGACUUGUGACCC	the Calcineurin-NFAT Pathway[41]
Sirt1	NM_001159589.2	sirtuin 1	Position 451-457 of Sirt1 3' UTR	5' ...CAGUUAACUUUUUAAACACUGGC... 3' CUUGUCCAUCAGACUUGUGACCC	the ERR transcriptional pathway[42]
Hif1a	NM_001313919.1	hypoxia inducible factor 1 subunit alpha	Position 237-243 of Hif1a 3' UTR	5' ...GUUGGUUAUUUUUGGACACUGGU... 3' CUUGUCCAUCAGACUUGUGACCC	HIF1α-PPARγ glycolytic and lipid anabolic pathways[43]
Ppard	NM_011145.3	peroxisome proliferator activated receptor delta	Position 902-908 of Ppard 3' UTR	5' ...CCCGGUGUAGCCAUGACACUGGC... 3' CUUGUCCAUCAGAUUUGUGACCC	cardiac glucose utilization and metabolic regulatory[44]
Gsk3b	NM_001347232.1	glycogen synthase kinase 3 beta	Position 61-67 of Gsk3b 3' UTR	5' ...GAGUGCCACUCAGCAACACUGGU... 3' CUUGUCCAUCAGACUUGUGACCC	mToR signaling and inhibit autophagy pathway[45]
			Position 3781-3787 of Gsk3b 3' UTR	5' ...CCUGUGGACGUAAAGACACUGGC... 3' CUUGUCCAUCAGACUUGUGACCC	

The results of increased glucose oxidation, FAO and OXPHOS, were in line with the activation of the PGC-1/ERR axis.

Previous studies show that PGC-1α directly coactivates ERRα and that ERRα is required for PGC-1α function in mitochondrial metabolism.[31,32] ERRα is a key regulator in energy substrate oxidation, OXPHOS, and ATP synthesis. The ERRα KO mice developed heart failure after TAC, with reduced mitochondrial metabolism and ATP synthesis.[33] In contrast, overexpression of ERRα activates PPARα and upregulates most genes involved in mitochondrial energy-producing pathways in cardiomyocytes.[34] Our study shows that the expression of both PGC-1α and ERRα increased in anti-miR-199a-treated hearts and that the expression of the downstream mitochondrial metabolism pathway was upregulated, which indicates that the PGC-1/ERR axis is the possible underlying protective mechanism of anti-miR-199a treatment.

Interestingly, PGC-1α can be activated by exercise and promote cardiac mitochondrial biogenesis.[27,35] PGC-1α is also involved in physiological cardiac hypertrophy in miR-199a sponge transgenic mice.[23] There are two possible explanations of why miR-199 knockdown plays a different role under the physiological and pathological conditions. First, the method we used to inhibit miR-199a is different from that in the study by Li et al.[23] Li et al. used sponge RNA to inhibit the expression of miR-199a, which also inhibited miR-199b expression. However, we used TuDs structure with two miR-199a binding sties and no inhibition effect on miR-199b. Second, the regulation of PGC-1α itself is sophisticated in a developmental stage-dependent manner.[28] The AAV9 technology we used only drives the expression of anti-miR-199a TuDs postnatally, while the genetic knockin of miR-199a sponge works in the whole fetal development period. However, the underlying mechanism of miR-199a-PCG-1α should be further investigated through the study of different cardiomyocyte gene expression and mitochondrial metabolomics.

el Azzouzi et al.[4] also proved that the inhibition of miR-199a and miR-214 using the miRNA antagomir improved cardiac function and restored mitochondrial FAO by targeting PPARδ. Our results are partly in line with their study. The expression of glycolysis genes, FAO genes, and important transcription factors involved in mitochondrial metabolism returned to a normal level compared with that in the cardiac hypertrophy model. However, PPARδ was not significantly changed in cardiac hypertrophy after anti-miR-199a treatment. The main contribution to their recovered phenotype is the inhibition of miR-214 by the antagomir.[4] In addition, the AAV9 delivery system achieved cardiac-specific, highly efficient, and long-term inhibition, which is superior to the miRNA antagomir. This may explain why our results of anti-miR-199a treatment for cardiac hypertrophy are more profound. These advantages also make AAV a popular delivery method of miRNA either in mechanistic studies or therapeutic effects on cardiovascular diseases.[3,7,8,13–15]

In pressure-overload cardiac hypertrophy, mitochondrial metabolism usually shifts from FAO to glucose utilization. However, metabolic alterations also depend on the animal models, experimental settings, stage and severity of cardiac hypertrophy and dysfunction, and different pathological stimuli.[36] Decreased glycolysis also can be detected in abdominal aortic constriction-induced cardiac hypertrophy mice[37] and ISO-induced cardiac hypertrophy rats.[38] The cardiac insulin resistance in different cardiac hypertrophy models may explain the different glycolysis alterations in our model and the previous ones.

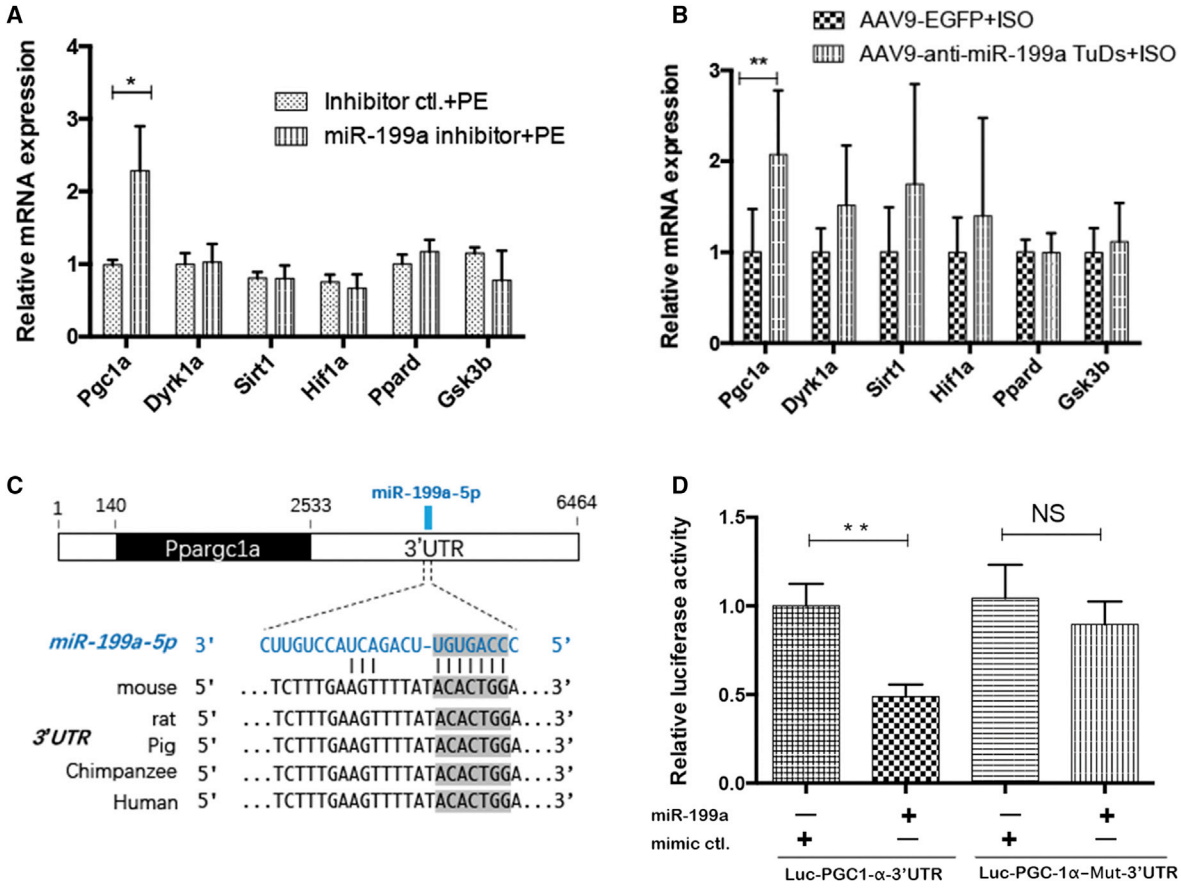

Figure 5. Validation of PGC-1α as a target of miR-199a in cardiac hypertrophy

(A) The expression of six predicted targets of miR-199a in hypertrophic NRVMs with and without miR-199a inhibitor treatment (n = 3). (B) The expression of six predicted targets of miR-199a in cardiac hypertrophy mice and the anti-miR-199a-treated mice (n = 8). (C) Schematic representation of genomic localization of miR-199a binding site in the 3′UTR of Ppargc1a gene and the conserved seed sequences in different species. (D) Dual luciferase activity assay of H293T cells co-transfected miR-199a mimic or mimic control with Luc-PGC-1α-3′UTR reporter plasmid or Luc-PGC-1α-Mut-3′UTR plasmid (n = 4). *p < 0.05, **p < 0.01.

There are several limitations in the present study. First, except for PGC-1α, there may be other contributing targets involved in the regulation of the PGC-1/ERR axis and the related mitochondrial metabolic pathway. A more comprehensive, high-throughput target study may discover new targets. Second, we did not record the dynamic change in anti-miR-199a-treated NRVMs by live cell imaging or Seahorse metabolism analysis, which generate more reliable information on mitochondrial metabolism. Third, the cardiac hypertrophy model induced by ISO injection is mainly generated through neurohormonal stress. Other cardiac hypertrophy models, such as TAC, should be studied. These topics warrant further investigation.

In conclusion, the current study reveals the important regulatory role of miR-199a in cardiac hypertrophy and highlights the efficiency and usefulness of an AAV-mediated miRNA delivery system. Further experiments regarding the mitochondrial metabolism pathway are still required to elucidate the specific mechanism and gain more molecular and functional insight.

MATERIALS AND METHODS

Cardiac hypertrophy model and echocardiographic measurement

Thirty-two C57BL/6 adult male mice (25–30 g) were used for the cardiac hypertrophy model. The establishment of a cardiac hypertrophy model has been previously described in detail.[39] In brief, mice were treated with isoproterenol (ISO, Sigma-Aldrich, St. Louis, MO, USA) to induce cardiac hypertrophy. ISO was dissolved in sterile saline and was injected intraperitoneally (60 mg/kg/day) once daily for 14 consecutive days.

Cardiac function was measured by a Vivid 7 ultrasound system (GE Healthcare, Horten, Norway) with a 13 MHz i13L cardiac transducer. Two-dimensional M-mode tracings were used to measure left ventricular internal dimension in diastole (LVIDd), left ventricular internal dimension in systole (LVIDs), and the percentages of LVEF and LVFS. All mice were sacrificed 3 weeks after the final injection of

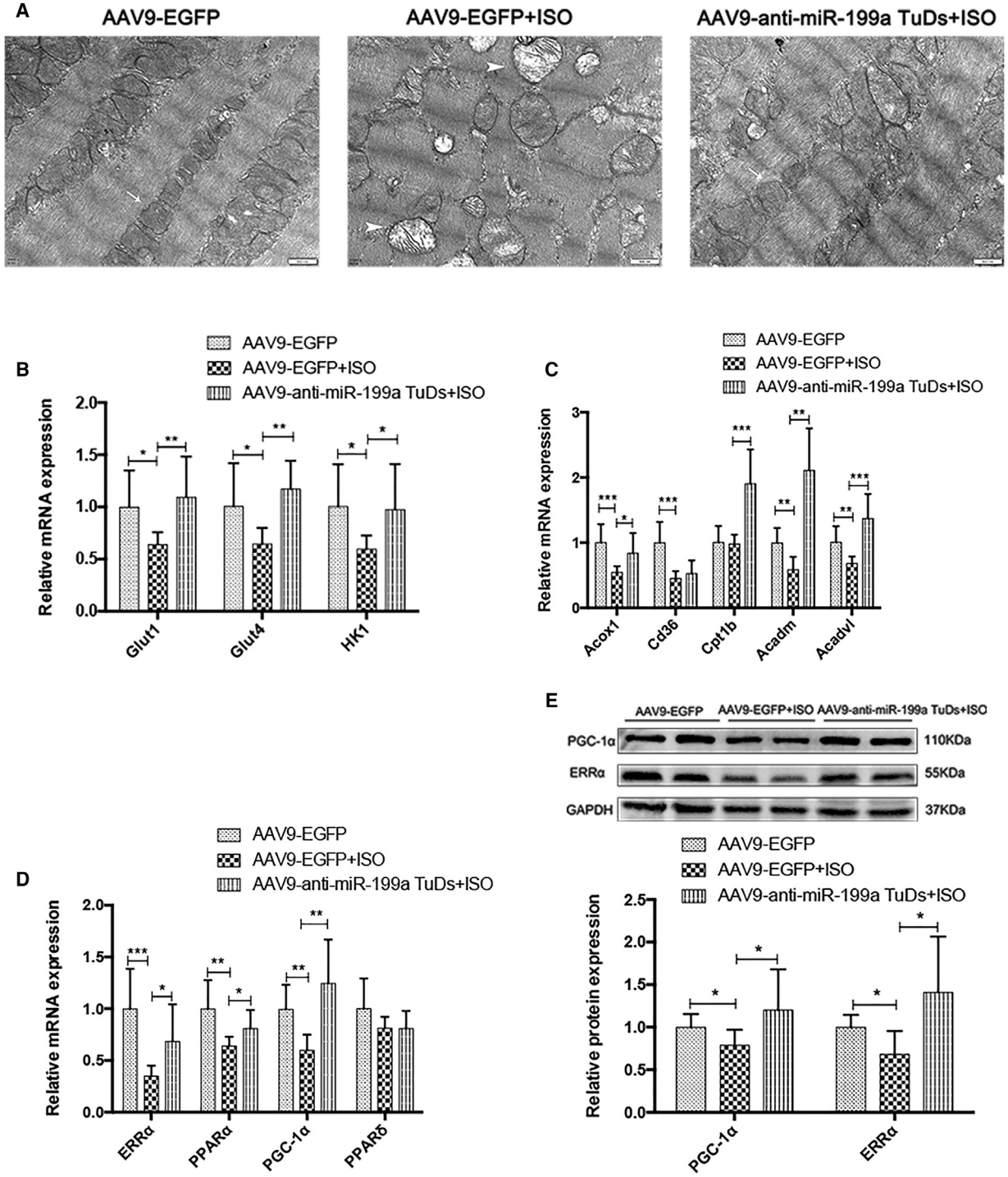

Figure 6. The disrupted mitochondrial ultrastructure and the altered genes related to mitochondrial metabolism are recovered by anti-miR-199a treatment

(A) Representative transmission electron microscopy (TEM) images in control, cardiac hypertrophy mice, and the anti-miR-199a-treated mice. Scale bars, 500 nm. Arrowhead, normal mitochondrial ultrastructure; arrow, disrupted mitochondrial ultrastructure (n = 3). (B) The expression of representative genes in glycolysis in each mouse group (n = 8). (C) The expression of representative genes in fatty acid oxidation (FAO) in each mouse group (n = 8). (D) The expression of important transcription factors involved in the mitochondrial metabolism in each mouse group (n = 8). (E) Representative western blot results and the relative protein expression of ERRα and PGC-1α in each mouse group (n = 6). *$p < 0.05$, **$p < 0.01$, ***$p < 0.001$.

ISO. The Institutional Animal Care and Use Committee of Sichuan University approved all the above experiments.

AAV9-anti-miR-199a TuDs cloning, virus packaging, and systemic delivery

We generated AAV9-U6-anti-miR-199a TuDs-cTNT-EGFP (AAV9-anti-miR-199a TuDs) from AAV9-U6-gRNA-cTNT-EGFP. AAV9-cTNT-EGFP (AAV9-EGFP) was used as a control (AAV9-U6-gRNA-cTNT-EGFP and AAV9-cTNT-EGFP plasmids were a gift from Yuxuan, Guo in William Pu's lab[40]). Anti-miR-199a TuDs contain two single-stranded miR-199a-5p binding sites flanked by double-stranded stems that generate a stable hairpin structure (Figure S4). The design of anti-miR-199a TuDs was based on a previous report.[17] The anti-miR-199a TuDs RNA was cloned into the AAV9-U6-gRNA-cTNT-EGFP plasmid using AgeI and RsrII restriction enzymes. The design of anti-miR-199a TuDs and the schematic diagram of the AAV9-anti-miR-199a TuDs plasmid are shown in detail in Figure S4.

The AAV9 virus was produced using a previous protocol.[40] In brief, the AAV-ITR plasmid (AAV9-anti-miR-199a TuDs or AAV9-cTNT-EGFP) and the AAV9-Rep-Cap and pHelper (pAd-deltaF6, Penn Vector Core, Philadelphia, PA, USA) plasmids were co-transfected into H293T cells. Three days later, cells were collected and lysed. AAV9 was purified and concentrated by gradient ultracentrifugation. The titer of AAV viral particles was quantified by real-time PCR. The viral preparations had titers between 1×10^{13} and 1×10^{14} Vg/mL. The AAV9-anti-miR-199a TuDs or AAV9-cTNT-EGFP virus was injected into 1-day-old (P1) pups of C57BL/6 mice subcutaneously at 1×10^{11} Vg per mouse.

Histological analysis, immunostaining, and microscopy imaging

Freshly dissected heart tissues were fixed in 4% paraformaldehyde overnight and then embedded in paraffin. The myocardial sections (5 μm) were stained with hematoxylin and eosin (H&E) for heart morphology, Masson's trichrome for cardiac fibrosis, or terminal deoxynucleotidyl transferase-mediated nick-end labeling (TUNEL, DeadEnd Fluorometric TUNEL System, Promega, Madison, WI, USA) for the detection of apoptosis. Images were viewed and captured by a ZEISS Axio Imager 2 microscope (Jena, Germany).

For immunostaining, heart tissues were embedded in tissue freezing medium (O.C.T. Compound, VWR, Torrance, CA, USA). Heart sections (5–6 μm) were incubated with primary antibodies at 4°C overnight and secondary antibodies for 2 h. The primary antibody was used as follows: anti-sarcomeric alpha actinin antibody (SAA, 1:200, ab9465, Abcam, Cambridge, MA, USA), WGA (Alexa Fluor 647 Conjugate, 1:400, W32466, Invitrogen). DAPI (62247, Invitrogen) was used to stain the nuclei. Immunostaining images were captured by an Olympus FV1000 confocal microscope (Tokyo, Japan). ImageJ software was used for all image analyses.

TEM imaging

The isolated mouse hearts were immersed in stationary liquid (pH 7.3) containing 3% glutaraldehyde. Tissue samples were then fixed in 2% osmic acid (OsO_4, Sigma-Aldrich) in phosphate-buffered solution. After dehydration with a concentration gradient of acetone solutions, tissues were then embedded in Epon (Epon 812, Sigma-Aldrich). Ultrathin sections (50 nm) were cut by microtome, mounted onto formvar-coated slot grids, and stained with uranyl acetate (Zhongjingkeyi, Beijing, China) and lead citrate (Zhongjingkeyi, Beijing, China) at room temperature. Images were captured by a JEM-1400PLUS electron microscope (Tokyo, Japan).

Primary culture of NRVMs, hypertrophic model, and miR-199a treatment

NRVMs were prepared according to the instructions of the neonatal cardiomyocyte isolation kit (nc-6031, Cellutron, Baltimore, MD, USA). Primary cardiomyocytes were isolated by enzymatic disassociation of P1 neonatal rat hearts. Cells were plated on SureCoat solution (sc-9035, Cellutron) coated plates in NS medium (m-8031, with serum, Cellutron). After plating overnight, the cells were changed to NW medium (m-8032, serum-free, Cellutron).

Then, 50 nM (final concentration) miR-199a mimic or 100 nM (final concentration) miR-199a inhibitor and control oligonucleotide (Ribobio, Guangzhou, China) were transfected into cardiomyocytes using Lipofectamine RNAiMAX transfection reagent (Invitrogen, Carlsbad, CA, USA). Twenty-four hours later, the cells were treated with 20 μM hypertrophic agent, phenylephrine (PE, Sigma-Aldrich). Cells were harvested 24 h after PE treatment for RNA isolation or 48 h after PE treatment for immunostaining.

RNA-seq, GO and KEGG pathway analyses, and miRNA database analysis

Three biological replicates of RNA samples from each group were prepared for RNA-seq. RNA-seq experiments were performed by Novogene (Beijing, China). In brief, RNA sequencing was performed on an Illumina NovaSeq 6000 platform (Illumina), and 150 bp paired-end reads were generated. For the data analysis, raw data in fastq format were first processed through in-house Perl scripts. Clean data were obtained by removing reads containing adapters, reads containing poly-N, and low-quality reads from raw data. *Mus musculus* GRCm38 (mm10) was the reference genome used, and gene model annotation files were downloaded from the genome website directly.

The index of the reference genome was built using Hisat2 v2.0.5, and paired-end clean reads were aligned to the reference genome using Hisat2 v2.0.5. Differential expression analysis of two conditions/groups (two biological replicates per condition) was performed using the DESeq2 R package (1.16.1). The p values were adjusted using the Benjamini and Hochberg method. GO enrichment and KEGG pathway analyses were implemented using the clusterProfiler R package. The RNA-seq data have been deposited in the GenBank Database (GenBank: GSE155545).

To predict the mRNA targets of miR-199a, we used TargetScan v7.2 (http://www.targetscan.org/) and TarBase v7.0 (http://diana.imis.athena-innovation.gr/DianaTools/index.php?r=tarbase/index).

Enzyme-linked immunosorbent assay (ELISA)

Same volumes of plasma samples from mice in each group were used to measure the levels of the inflammatory cytokines IL-1β, IL-6, and tumor necrosis factor alpha (TNF-α) using the corresponding ELISA kits (CME0015, CME0006, CME0004, 4A Biotech Co., Beijing, China) according to the manufacturers' instructions.

RNA extraction and real-time PCR

Hearts were frozen in liquid nitrogen and stored at −80°C. Total RNA was extracted from cardiac samples using a Total RNA Kit II (Omega, Norcross, GA, USA). RNA (0.5 μg) was reverse transcribed into cDNA using an iScript cDNA Synthesis Kit (Bio-Rad, Hercules, CA, USA). For miRNA detection, RNA was reverse transcribed into cDNA using the miRNA qRT-PCR Starter Kit (Ribobio, Guangzhou, China). Real-time PCR was performed with a CFX96 Real-Time System using SYBR Green (Bio-Rad, Hercules, CA, USA).

The reverse transcription (RT) and PCR primers for miR-199a, miR-199b, and the U6 control were from the primer set (Ribobio, Guangzhou, China) according to the accession number in the miRBase database (http://www.mirbase.org). The primer sequences for other mRNAs are listed in Table S2.

Western blot

Heart tissues were lysed in a RIPA lysis buffer system (Beyotime, Shanghai, China) with phenylmethanesulfonylfluoride (PMSF, Beyotime). Total protein concentrations were normalized using a BCA Protein Assay Kit (23227, Thermo Scientific, Rockford, IL, USA). Lysates were subsequently separated by 10% SDS/PAGE gels, transferred to PVDF membranes (IPVH00010, Millipore, Darmstadt, Germany), and blocked in 5% nonfat milk in TBST for 1 h. Then, membranes were incubated with the following antibodies overnight at 4°C: anti-PGC1 alpha antibody (ab54481, Abcam), anti-ERR alpha antibody (ab76228, Abcam), and anti-GAPDH loading control (ab9485, Abcam). Proteins were visualized by ECL Plus western blot detection reagents (Beyotime, Shanghai, China).

Luciferase reporter assay

A total of 50 ng of wild-type Luc-PGC-1α-3′UTR construct, mutant Luc-PGC-1α-Mut-3′UTR construct, 10 nM miR-199a mimic, or negative control was transfected into H293T cells by Lipofectamine 3000 (Invitrogen, Carlsbad, CA). Forty-eight hours after transfection, luciferase activities were measured using a dual luciferase reporter assay system from triplicate transfected wells.

Statistical analysis

Data are shown as the mean ± SD. The significance of intergroup differences was tested using Student's t test or the Mann-Whitney test as indicated in SPSS v.25.0 software (IBM, Armonk, NY, USA). $p < 0.05$ was considered statistically significant.

SUPPLEMENTAL INFORMATION

Supplemental Information can be found online at https://doi.org/10.1016/j.omtn.2020.11.007.

ACKNOWLEDGMENTS

The authors are grateful to Yuxuan Guo, Donghui Zhang, and other members of the William Pu lab of Boston Children's Hospital for their theoretical and technical help; to Xiaoyun Hu, Zhan-Peng Huang, and other members of the Da-Zhi Wang lab of Boston Children's Hospital for their theoretical and technical help; and for the support from the China Scholarship Council (CSC) during the visit (H.Y.) to the Boston Children's Hospital, Harvard Medical School. This work was funded by the National Natural Science Foundation of China (81671702), the China Postdoctoral Science Foundation (2019M653422), and the Post-Doctor Research Project, West China Hospital, Sichuan University (2018HXBH035).

AUTHOR CONTRIBUTIONS

H.Y., H.W., X.Z., J.H., Y. Li, D.-Z.W., F.Y., and Y. Luo designed and performed experiments. H.Y., Y. Li, K.Z., and Y.H. analyzed and interpreted the data. H.Y. analyzed the RNA-seq data and wrote the manuscript. F.Y. and Y. Luo revised the manuscript. H.Y., F.Y., and Y. Luo supplied funding and supervised the work. All authors read and approved the final manuscript.

DECLARATION OF INTERESTS

The authors declare no competing interests.

REFERENCES

1. Nakamura, M., and Sadoshima, J. (2018). Mechanisms of physiological and pathological cardiac hypertrophy. Nat. Rev. Cardiol. *15*, 387–407.

2. Liu, B.L., Cheng, M., Hu, S., Wang, S., Wang, L., Tu, X., Huang, C.X., Jiang, H., and Wu, G. (2018). Overexpression of miR-142-3p improves mitochondrial function in cardiac hypertrophy. Biomed. Pharmacother. *108*, 1347–1356.

3. Qiu, Y., Cheng, R., Liang, C., Yao, Y., Zhang, W., Zhang, J., Zhang, M., Li, B., Xu, C., and Zhang, R. (2020). MicroRNA-20b Promotes Cardiac Hypertrophy by the Inhibition of Mitofusin 2-Mediated Inter-organelle Ca^{2+} Cross-Talk. Mol. Ther. Nucleic Acids *19*, 1343–1356.

4. el Azzouzi, H., Leptidis, S., Dirkx, E., Hoeks, J., van Bree, B., Brand, K., McClellan, E.A., Poels, E., Sluimer, J.C., van den Hoogenhof, M.M., et al. (2013). The hypoxia-inducible microRNA cluster miR-199a∼214 targets myocardial PPARδ and impairs mitochondrial fatty acid oxidation. Cell Metab. *18*, 341–354.

5. Dai, D.F., Johnson, S.C., Villarin, J.J., Chin, M.T., Nieves-Cintrón, M., Chen, T., Marcinek, D.J., Dorn, G.W., 2nd, Kang, Y.J., Prolla, T.A., et al. (2011). Mitochondrial oxidative stress mediates angiotensin II-induced cardiac hypertrophy and Galphaq overexpression-induced heart failure. Circ. Res. *108*, 837–846.

6. Wang, T., Zhai, M., Xu, S., Ponnusamy, M., Huang, Y., Liu, C.Y., Wang, M., Shan, C., Shan, P.P., Gao, X.Q., et al. (2020). NFATc3-dependent expression of miR-153-3p promotes mitochondrial fragmentation in cardiac hypertrophy by impairing mitofusin-1 expression. Theranostics *10*, 553–566.

7. Oh, J.G., Watanabe, S., Lee, A., Gorski, P.A., Lee, P., Jeong, D., Liang, L., Liang, Y., Baccarini, A., Sahoo, S., et al. (2018). miR-146a Suppresses SUMO1 Expression and Induces Cardiac Dysfunction in Maladaptive Hypertrophy. Circ. Res. *123*, 673–685.

8. Nie, X., Fan, J., Li, H., Yin, Z., Zhao, Y., Dai, B., Dong, N., Chen, C., and Wang, D.W. (2018). miR-217 Promotes Cardiac Hypertrophy and Dysfunction by Targeting PTEN. Mol. Ther. Nucleic Acids *12*, 254–266.

9. Tian, C., Hu, G., Gao, L., Hackfort, B.T., and Zucker, I.H. (2020). Extracellular vesicular MicroRNA-27a* contributes to cardiac hypertrophy in chronic heart failure. J. Mol. Cell. Cardiol. *143*, 120–131.

10. Chu, Q., Li, A., Chen, X., Qin, Y., Sun, X., Li, Y., Yue, E., Wang, C., Ding, X., Yan, Y., et al. (2018). Overexpression of miR-135b attenuates pathological cardiac hypertrophy by targeting CACNA1C. Int. J. Cardiol. *269*, 235–241.

11. Zaglia, T., Ceriotti, P., Campo, A., Borile, G., Armani, A., Carullo, P., Prando, V., Coppini, R., Vida, V., Stølen, T.O., et al. (2017). Content of mitochondrial calcium uniporter (MCU) in cardiomyocytes is regulated by microRNA-1 in physiologic and pathologic hypertrophy. Proc. Natl. Acad. Sci. USA *114*, E9006–E9015.

12. Xie, J., Burt, D.R., and Gao, G. (2015). Adeno-associated virus-mediated microRNA delivery and therapeutics. Semin. Liver Dis. *35*, 81–88.

13. Li, H., Fan, J., Zhao, Y., Zhang, X., Dai, B., Zhan, J., Yin, Z., Nie, X., Fu, X.D., Chen, C., and Wang, D.W. (2019). Nuclear miR-320 Mediates Diabetes-Induced Cardiac Dysfunction by Activating Transcription of Fatty Acid Metabolic Genes to Cause Lipotoxicity in the Heart. Circ. Res. *125*, 1106–1120.

14. Gao, F., Kataoka, M., Liu, N., Liang, T., Huang, Z.P., Gu, F., Ding, J., Liu, J., Zhang, F., Ma, Q., et al. (2019). Therapeutic role of miR-19a/19b in cardiac regeneration and protection from myocardial infarction. Nat. Commun. *10*, 1802.

15. Hou, Z., Qin, X., Hu, Y., Zhang, X., Li, G., Wu, J., Li, J., Sha, J., Chen, J., Xia, J., et al. (2019). Longterm Exercise-Derived Exosomal miR-342-5p: A Novel Exerkine for Cardioprotection. Circ. Res. *124*, 1386–1400.

16. Zacchigna, S., Zentilin, L., and Giacca, M. (2014). Adeno-associated virus vectors as therapeutic and investigational tools in the cardiovascular system. Circ. Res. *114*, 1827–1846.

17. Xie, J., Ameres, S.L., Friedline, R., Hung, J.H., Zhang, Y., Xie, Q., Zhong, L., Su, Q., He, R., Li, M., et al. (2012). Long-term, efficient inhibition of microRNA function in mice using rAAV vectors. Nat. Methods *9*, 403–409.

18. Yan, H., Li, Y., Wang, C., Zhang, Y., Liu, C., Zhou, K., and Hua, Y. (2017). Contrary microRNA Expression Pattern Between Fetal and Adult Cardiac Remodeling: Therapeutic Value for Heart Failure. Cardiovasc. Toxicol. *17*, 267–276.

19. Zhang, H., Li, S., Zhou, Q., Sun, Q., Shen, S., Zhou, Y., Bei, Y., and Li, X. (2016). Qiliqiangxin Attenuates Phenylephrine-Induced Cardiac Hypertrophy through Downregulation of MiR-199a-5p. Cell. Physiol. Biochem. *38*, 1743–1751.

20. Song, X.W., Li, Q., Lin, L., Wang, X.C., Li, D.F., Wang, G.K., Ren, A.J., Wang, Y.R., Qin, Y.W., Yuan, W.J., and Jing, Q. (2010). MicroRNAs are dynamically regulated in hypertrophic hearts, and miR-199a is essential for the maintenance of cell size in cardiomyocytes. J. Cell. Physiol. *225*, 437–443.

21. Rane, S., He, M., Sayed, D., Vashistha, H., Malhotra, A., Sadoshima, J., Vatner, D.E., Vatner, S.F., and Abdellatif, M. (2009). Downregulation of miR-199a derepresses hypoxia-inducible factor-1alpha and Sirtuin 1 and recapitulates hypoxia preconditioning in cardiac myocytes. Circ. Res. *104*, 879–886.

22. Li, Z., Song, Y., Liu, L., Hou, N., An, X., Zhan, D., Li, Y., Zhou, L., Li, P., Yu, L., et al. (2017). miR-199a impairs autophagy and induces cardiac hypertrophy through mTOR activation. Cell Death Differ. *24*, 1205–1213.

23. Li, Z., Liu, L., Hou, N., Song, Y., An, X., Zhang, Y., Yang, X., and Wang, J. (2016). miR-199-sponge transgenic mice develop physiological cardiac hypertrophy. Cardiovasc. Res. *110*, 258–267.

24. Schilling, J., and Kelly, D.P. (2011). The PGC-1 cascade as a therapeutic target for heart failure. J. Mol. Cell. Cardiol. *51*, 578–583.

25. Kärkkäinen, O., Tuomainen, T., Mutikainen, M., Lehtonen, M., Ruas, J.L., Hanhineva, K., and Tavi, P. (2019). Heart specific PGC-1α deletion identifies metabolome of cardiac restricted metabolic heart failure. Cardiovasc. Res. *115*, 107–118.

26. Arany, Z., Novikov, M., Chin, S., Ma, Y., Rosenzweig, A., and Spiegelman, B.M. (2006). Transverse aortic constriction leads to accelerated heart failure in mice lacking PPAR-gamma coactivator 1alpha. Proc. Natl. Acad. Sci. USA *103*, 10086–10091.

27. Lehman, J.J., Barger, P.M., Kovacs, A., Saffitz, J.E., Medeiros, D.M., and Kelly, D.P. (2000). Peroxisome proliferator-activated receptor gamma coactivator-1 promotes cardiac mitochondrial biogenesis. J. Clin. Invest. *106*, 847–856.

28. Russell, L.K., Mansfield, C.M., Lehman, J.J., Kovacs, A., Courtois, M., Saffitz, J.E., Medeiros, D.M., Valencik, M.L., McDonald, J.A., and Kelly, D.P. (2004). Cardiac-specific induction of the transcriptional coactivator peroxisome proliferator-activated receptor gamma coactivator-1alpha promotes mitochondrial biogenesis and reversible cardiomyopathy in a developmental stage-dependent manner. Circ. Res. *94*, 525–533.

29. Pereira, R.O., Wende, A.R., Crum, A., Hunter, D., Olsen, C.D., Rawlings, T., Riehle, C., Ward, W.F., and Abel, E.D. (2014). Maintaining PGC-1α expression following pressure overload-induced cardiac hypertrophy preserves angiogenesis but not contractile or mitochondrial function. FASEB J. *28*, 3691–3702.

30. Karamanlidis, G., Garcia-Menendez, L., Kolwicz, S.C., Jr., Lee, C.F., and Tian, R. (2014). Promoting PGC-1α-driven mitochondrial biogenesis is detrimental in pressure-overloaded mouse hearts. Am. J. Physiol. Heart Circ. Physiol. *307*, H1307–H1316.

31. Huss, J.M., Kopp, R.P., and Kelly, D.P. (2002). Peroxisome proliferator-activated receptor coactivator-1alpha (PGC-1alpha) coactivates the cardiac-enriched nuclear receptors estrogen-related receptor-alpha and -gamma. Identification of novel leucine-rich interaction motif within PGC-1alpha. J. Biol. Chem. *277*, 40265–40274.

32. Rangwala, S.M., Li, X., Lindsley, L., Wang, X., Shaughnessy, S., Daniels, T.G., Szustakowski, J., Nirmala, N.R., Wu, Z., and Stevenson, S.C. (2007). Estrogen-related receptor alpha is essential for the expression of antioxidant protection genes and mitochondrial function. Biochem. Biophys. Res. Commun. *357*, 231–236.

33. Huss, J.M., Imahashi, K., Dufour, C.R., Weinheimer, C.J., Courtois, M., Kovacs, A., Giguère, V., Murphy, E., and Kelly, D.P. (2007). The nuclear receptor ERRalpha is required for the bioenergetic and functional adaptation to cardiac pressure overload. Cell Metab. *6*, 25–37.

34. Huss, J.M., Torra, I.P., Staels, B., Giguère, V., and Kelly, D.P. (2004). Estrogen-related receptor alpha directs peroxisome proliferator-activated receptor alpha signaling in the transcriptional control of energy metabolism in cardiac and skeletal muscle. Mol. Cell. Biol. *24*, 9079–9091.

35. Safdar, A., Little, J.P., Stokl, A.J., Hettinga, B.P., Akhtar, M., and Tarnopolsky, M.A. (2011). Exercise increases mitochondrial PGC-1alpha content and promotes nuclear-mitochondrial cross-talk to coordinate mitochondrial biogenesis. J. Biol. Chem. *286*, 10605–10617.

36. Tran, D.H., and Wang, Z.V. (2019). Glucose Metabolism in Cardiac Hypertrophy and Heart Failure. J. Am. Heart Assoc. *8*, e012673.

37. Zhang, L., Jaswal, J.S., Ussher, J.R., Sankaralingam, S., Wagg, C., Zaugg, M., and Lopaschuk, G.D. (2013). Cardiac insulin-resistance and decreased mitochondrial energy production precede the development of systolic heart failure after pressure-overload hypertrophy. Circ. Heart Fail. *6*, 1039–1048.

38. Heather, L.C., Catchpole, A.F., Stuckey, D.J., Cole, M.A., Carr, C.A., and Clarke, K. (2009). Isoproterenol induces in vivo functional and metabolic abnormalities: similar to those found in the infarcted rat heart. J. Physiol. Pharmacol. *60*, 31–39.

39. Huang, Z.P., Chen, J., Seok, H.Y., Zhang, Z., Kataoka, M., Hu, X., and Wang, D.Z. (2013). MicroRNA-22 regulates cardiac hypertrophy and remodeling in response to stress. Circ. Res. *112*, 1234–1243.

40. Guo, Y., VanDusen, N.J., Zhang, L., Gu, W., Sethi, I., Guatimosim, S., Ma, Q., Jardin, B.D., Ai, Y., Zhang, D., et al. (2017). Analysis of Cardiac Myocyte Maturation Using CASAAV, a Platform for Rapid Dissection of Cardiac Myocyte Gene Function In Vivo. Circ. Res. *120*, 1874–1888.

41. da Costa Martins, P.A., Salic, K., Gladka, M.M., Armand, A.S., Leptidis, S., el Azzouzi, H., Hansen, A., Coenen-de Roo, C.J., Bierhuizen, M.F., van der Nagel, R., et al. (2010). MicroRNA-199b targets the nuclear kinase Dyrk1a in an auto-amplification loop promoting calcineurin/NFAT signalling. Nat. Cell Biol. *12*, 1220–1227.

42. Oka, S., Alcendor, R., Zhai, P., Park, J.Y., Shao, D., Cho, J., Yamamoto, T., Tian, B., and Sadoshima, J. (2011). PPARα-Sirt1 complex mediates cardiac hypertrophy and failure through suppression of the ERR transcriptional pathway. Cell Metab. *14*, 598–611.

43. Krishnan, J., Suter, M., Windak, R., Krebs, T., Felley, A., Montessuit, C., Tokarska-Schlattner, M., Aasum, E., Bogdanova, A., Perriard, E., et al. (2009). Activation of a HIF1alpha-PPARgamma axis underlies the integration of glycolytic and lipid anabolic pathways in pathologic cardiac hypertrophy. Cell Metab. *9*, 512–524.

44. Burkart, E.M., Sambandam, N., Han, X., Gross, R.W., Courtois, M., Gierasch, C.M., Shoghi, K., Welch, M.J., and Kelly, D.P. (2007). Nuclear receptors PPARbeta/delta and PPARalpha direct distinct metabolic regulatory programs in the mouse heart. J. Clin. Invest. *117*, 3930–3939.

45. Zhai, P., Sciarretta, S., Galeotti, J., Volpe, M., and Sadoshima, J. (2011). Differential roles of GSK-3β during myocardial ischemia and ischemia/reperfusion. Circ. Res. *109*, 502–511.

OMTN, Volume *23*

Supplemental Information

Adeno-associated virus-mediated delivery of anti-miR-199a tough decoys attenuates cardiac hypertrophy by targeting *PGC-1alpha*

Hualin Yan, Hong Wang, Xiaoxia Zhu, Jianbo Huang, Yifei Li, Kaiyu Zhou, Yimin Hua, Feng Yan, Da-Zhi Wang, and Yan Luo

Table S1. Echocardiographic assessment of each mice group.

	AAV9-EGFP	AAV9-EGFP + ISO	AAV9-anti-miR-199a TuDs + ISO
LVIDd, mm	3.22±0.16	4.06±0.26**	3.30±0.13##
LVIDs, mm	1.87±0.18	2.78±0.22**	1.90±0.18##
LVEDV, μL	41.82±5.10	72.84±10.94**	44.25±4.36##
LVESV, μL	10.86±2.61	29.31±5.78**	11.35±2.59##
LVEF, %	80.84±6.39	59.92±7.71**	70.05±3.19##
LVFS, %	48.58±6.43	31.69±4.96**	38.73±2.54##
number of mice	8	8	8

Abbreviation: LVIDd, left ventricular internal dimension in diastole; LVIDs, left ventricular internal dimension in systole; LVEDV, left ventricular end-diastolic volume; LVESV, left ventricular end- systolic volume; LVEF, left ventricular ejection fraction; LVFS, left ventricular fractional shortening. *: $P<0.05$, **: $P<0.01$, AAV9- EGFP+ISO vs. AAV9-EGFP; #: $P<0.05$, ## $P<0.01$, AAV9-anti-miR-199a TuDs +ISO vs. AAV9-EGFP +ISO.

Table S2. The primer sequences for RT-qPCR

Target genes	Primer sequences (5'-3')
Nppa(ANP)	Forward: GGGCTCCTTCTCCATCACC
	Reverse: CTCCAATCCTGTCAATCCTACC
Nppb(BNP)	Forward: CTGAAGGTGCTGTCCCAGAT
	Reverse: GTTCTTTTGTGAGGCCTTGG
Myh7(β-MHC)	Forward: CTCAGAGCTCAAGCGGGATA
	Reverse: CCAGCCATCTCCTCTGTCA
Acta1	Forward: CAAAGACAAGCTGTGCTACGTG
	Reverse: GATGCTGTTGTAGGTGGTCTCA
Rps27a	Forward: ACTCCCAAGAAGAACAAGCATA
	Reverse: CAGTAAGTCAGACAACACTTGC
Rpl23	Forward: GGATTTCCCTGGGTCTTCCG
	Reverse: TTCAGCCGTCCCTTGATTCC
Mrps21	Forward: ATAAGTCGACGACGCTACTATG
	Reverse: GCCATTTCCATGTTGTAGATCC
Mrpl14	Forward: GAATGACCCCAAAGTTTGACTC
	Reverse: GCTGGTCGGGATAGGTATTTTA
Ndufa6	Forward: CTTAATGCAGCTGGATATCACG
	Reverse: TTTCCCTTAATGACCAGCAGAT
Ndufb3	Forward: CCCGAGGGCTGAGGGAT
	Reverse: TGCAAAGCCGCCCATG
Ndufb7	Forward: GCCGGACCTCGGCTTT
	Reverse: CTGGGCATCCATCATCTCTTG
Sdhb	Forward: CGCTGCCACACCATCATG
	Reverse: TTTCCGCAATCGCTTTCC
Uqcrh	Forward: AGGACGAACGAAAGATGCTCACTG
	Reverse: CGGGCCTTTACACACTTCTCCAG
Uqcrq	Forward: CGTTTGTAGTGGTCTACCTGAT
	Reverse: ATACATGGCTGGATTCTTCCTT
Cox4i1	Forward: TACTTCGGTGTGCCTTCGA
	Reverse: TGACATGGGCCACATCAG
Atp5l	Forward: TGCTGAAATCCCTACAGCTATT
	Reverse: GCACAGCTTCCTTAACTGTAAG
Ppard	Forward: TGGAGCTCGATGACAGTGAC
	Reverse: GTACTGGCTGTCAGGGTGGT
Ppara	Forward: ATGCCAGTACTGCCGTTTTC
	Reverse: GGCCTTGACCTTGTTCATGT
Ppargc1a(Pgc1a)	Forward: GGATATACTTTACGCAGGTCGA
	Reverse: CGTCTGAGTTGGTATCTAGGTC
Cd36(Fatp)	Forward: GAGCCTTCACTGTCTGTTGGAA
	Reverse: CTGCTACAGCCAGATTCAGAAC
Cpt1b	Forward: GGCACCTCTTCTGCCTTTAC

	Reverse: TTTGGGTCAAACATGCAGAT
Acox1	Forward: GGGAGTGCTACGGGTTACATG
	Reverse: CCGATATCCCCAACAGTGATG
Acadm	Forward: GATGCATCACCCTCGTGTAAC
	Reverse: AAGCCCTTTTCCCCTGAA
Acadvl	Forward: TTACATGCTGAGTGCCAACATG
	Reverse: CGCCTCCGAGCAAAAGATT
Esrra(ERRα)	Forward: GGCACAAGGAGGAGGAGGATGG
	Reverse: AGGCAGAGGCGTTTGGGTAGAG
Gsk3b	Forward: TGGTAGCATGAAAGTTAGCAGA
	Reverse: CTCTCGGTTCTTAAATCGCTTG
Slc2a1(Glut1)	Forward: GAAGAAGGTCACCATCTTGGAG
	Reverse: CGAAGATGCTCGTTGAGTAGTA
Slc2a4(Glut4)	Forward: TATTCAACCAGCATCTTCGAGT
	Reverse: GTCCAGCTCGTTCTACTAAGAG
Hk1	Forward: AGTGGAAGCCAGCTTTTTGA
	Reverse: TTCAGCAGCTTGACCACATC
Gapdh	Forward: TGTGTCCGTCGTGGATCTGA
	Reverse: CCTGCTTCACCACCTTCTTGA

Abbreviation: Nppa, natriuretic peptide type A; Nppb, natriuretic peptide type B; Myh7, myosin heavy chain 7; Acta1, actin alpha 1, skeletal muscle; Rps27a, ribosomal protein S27A; Rpl23, ribosomal protein L23; Mrps21, mitochondrial ribosomal protein S21; Mrpl14, mitochondrial ribosomal protein L14; Ndufa6, NADH:ubiquinone oxidoreductase subunit A6; Ndufb3, NADH:ubiquinone oxidoreductase subunit B3; Ndufb7, NADH:ubiquinone oxidoreductase subunit B7; Sdhb, succinate dehydrogenase complex, subunit B, iron sulfur (Ip); Uqcrh, ubiquinol-cytochrome c reductase hinge protein; Uqcrq, ubiquinol-cytochrome c reductase, complex III subunit VII; Cox4i1, cytochrome c oxidase subunit 4I1; Atp5l, ATP synthase, H+ transporting, mitochondrial F0 complex, subunit G; Ppard, peroxisome proliferator activated receptor delta; Ppara, peroxisome proliferator activated receptor alpha; Ppargc1a, peroxisome proliferative activated receptor, gamma, coactivator 1 alpha; Cd36, also known as fatty acid translocase (FAT); Acox1, acyl-Coenzyme A oxidase 1, palmitoyl; Acadm, acyl-Coenzyme A dehydrogenase, medium chain; Acadvl, acyl-Coenzyme A dehydrogenase, very long chain; Slc2a1, solute carrier family 2 member 1, also known as glucose transporter 1 (Glut1); Slc2a4, solute carrier family 2 member 4, also known as glucose transporter 4 (Glut4); Hk1, hexokinase 1; Gapdh, glyceraldehyde-3-phosphate dehydrogenase; Esrra, estrogen related receptor alpha; Gsk3b, glycogen synthase kinase 3 beta.

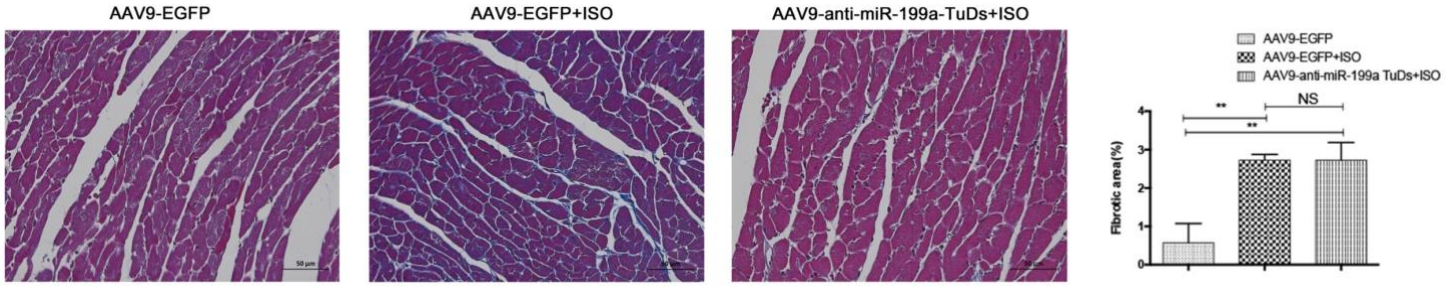

Figure S1. Masson staining of cardiac fibrosis of cardiomyocyte in each group. Bars, 50 μm. Fibrosis ratio is calculated by the ratio of the blue-stained interstitial fibrotic areas and the red-stained whole cardiomyocyte area. *: $P<0.05$, **: $P<0.01$, NS, not significant.

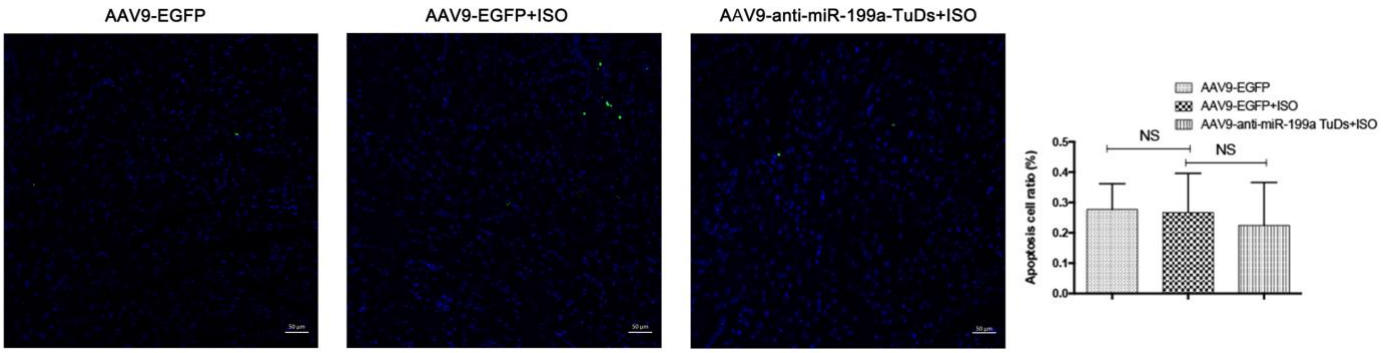

Figure S2. TUNEL detection of apoptosis of cardiomyocyte in each group. Blue, DAPI staining of nuclei; Green, cell apoptosis detected by TUNEL kit. Bars, 50 μm. Apoptosis cell ratio is calculated by the ratio of TUNEL positive cells and DAPI cells. TUNEL, terminal deoxynucleotidyl transferase-mediated nick-end labeling; NS, not significant.

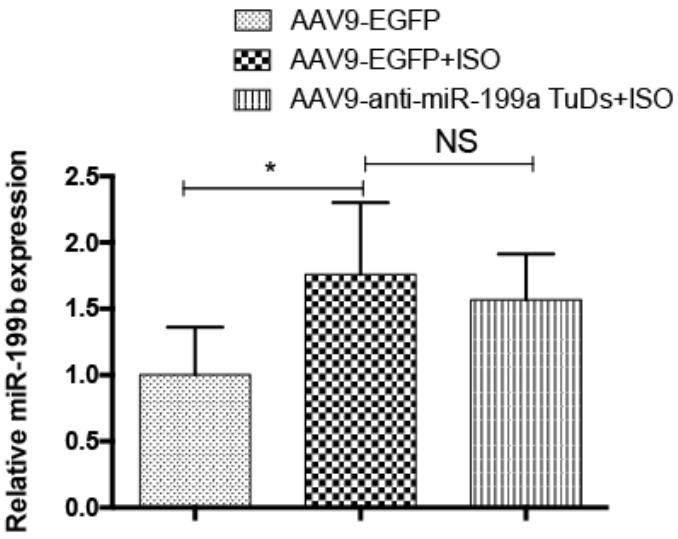

Figure S3. miR-199b expression level detected by real-time PCR. * $P < 0.05$.

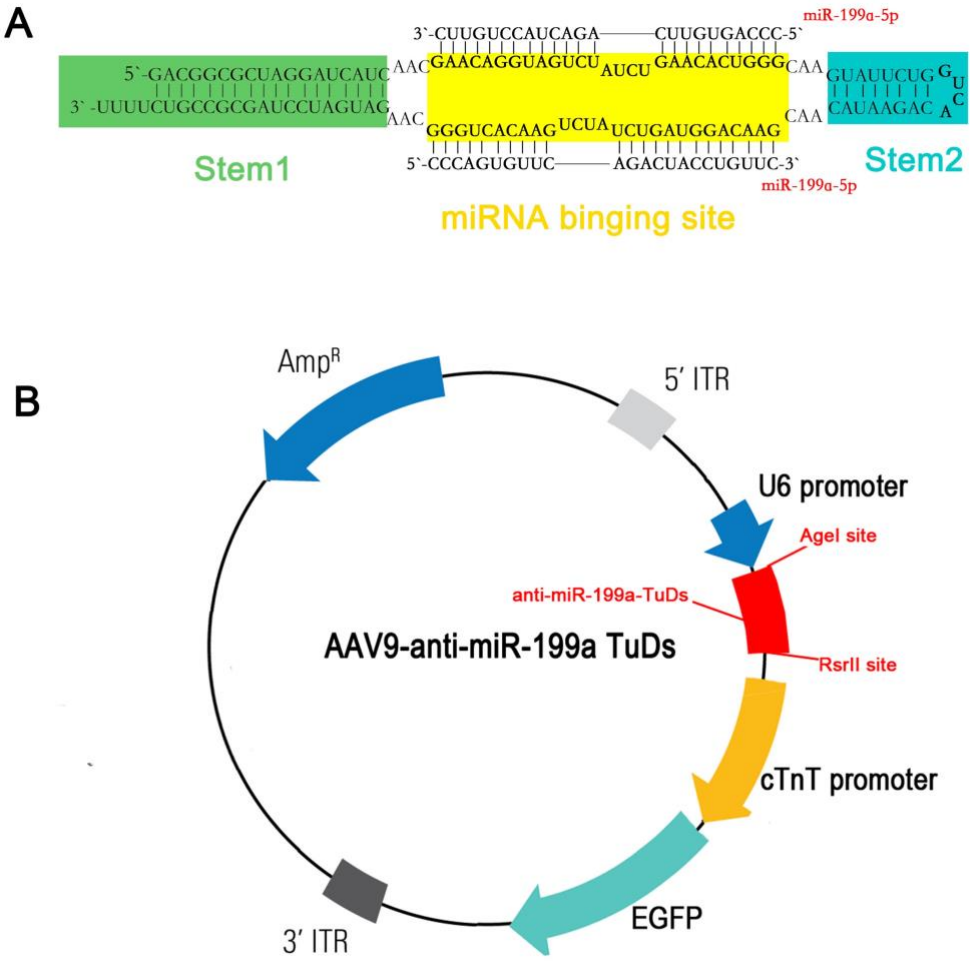

Figure S4. Schematic diagram of AAV9-anti-miR-199a TuDs plasmid. (A) the harpin structure of anti-miR-199a TuDs insert contains two single-stranded miR-199a-5p binding sites (yellow sequences) and two double-stranded stems (green and blue sequences). (B) AAV9-anti-miR-199a TuDs plasmid harbors the U6 promoter and the chicken cardiac TNT promoter, to generate anti-miR-199a TuDs and EGFP, respectively. ITR, inverted terminal repeat. TuDs, tough decoys.